Supplemental material

Supplemental introductory information

Human type 1 sigma receptor (sigma1-receptor; σ_1), at first cloned and functionally expressed by Kekuda et al. (*1*), is involved in a wide array of cellular functions such as biogenesis of lipid microdomains at the plasma membrane, the regulation of different receptors and ion channels as well as the modulation of calcium signaling. Despite the fact that the gene coding for σ_1 is located on chromosome 9 which is related to schizophrenia genetics, analyses of controls and schizophrenics show inconsistent results on a direct association between the σ_1 gene and schizophrenia (*2-5*). However, indirect modulation of several neurotransmitter systems by potent σ_1 agonists such as the selective serotonin reuptake inhibitor fluvoxamine is assumed to contribute to a therapeutic efficacy in patients with schizophrenia (*6*).

References to previous sigma$_1$ receptor ligands
^{18}F-FPS (*7*) (*8*) (*9*)
^{18}F-FBFPA (*10*)
^{18}F-FM-SA4503 (*11*)
^{11}C-SA4503 (*12, 13*)
^{18}F-labelled benzamides (*14*).

Supplement to Material and Methods

Synthesis of radiotracers
Confirmation of the enantiomeric purity of (*R*)-(+)- and (*S*)-(–)-^{18}F-fluspidine in the radiosynthetic process was achieved by chiral HPLC using a Reprosil Chiral-OM column (250×4.6 mm; 5 µm particle size; Dr. Maisch GmbH) and 95% n-hexane/5% isopropanol/0.05% diethyl amine (v/v/v) with a flow rate of 0.75 mL/min.

Animals and drugs
SA4503 was synthesized as dihydrochloride salt as previously described (*15*) and was characterized by reverse phase HPLC (> 97% pure), 1H NMR and 13C NMR (*16*). Characterization data were consistent with those obtained with previously synthesised materials (*16*).

Positron emission tomography
Twelve pigs were studied with PET under general anesthesia (0.5 % isoflurane in a gas mixture of 70 % nitrous oxide and 30 % oxygen via endotracheal tube using a volume-controlled ventilator). Pancuronium was infused at a rate of 0.3 mg/kg/h. Blood gases, end-tidal CO_2 and body temperature were continuously monitored.
PET imaging was performed with an ECAT EXACT HR+ (CTI/Siemens) scanner at a spatial resolution (transaxial) of 4-5 mm (*17*). Reconstruction of both PET scans was done using filtered back projection with a Hanning filter (cutoff frequency of 0.5). For attenuation and scatter correction, a transmission scan using three rotating ^{68}Ge rod sources was performed prior to the emission scan.

Metabolite analysis
After centrifugation about 1 ml plasma was obtained and plasma proteins were precipitated by addition of acetonitrile (plasma:acetonitrile = 1:2 v/v). Metabolite analysis was carried out by gradient HPLC in the following configuration: Hewlett-Packard 1100 quaternary gradient pump, autosampler (900 µl sample loop; injection volume 500-900 µl), UV detector (λ= 254 nm), all parts of the Hewlett-Packard 1100 system, and a flow scintillation analyzer (150 TR, Canberra Packard) with a PET flow cell (100 µl volume; energy window: 80 - 1750 keV). The analytes were separated on Merck RP-18e column (Purospher, 125x3 mm, 5 µm) at a temperature of 28 °C. A binary gradient was chosen at a flow rate of 0.75 ml/min (0-1 min 23 % B, 5-11 min 70 % B; total method time: 11 min). Mobile phase A consisted of 0.1 M ammonium formate, pH 7.0. Mobile phase B was MeCN.

Data analysis and model description
Radioactivity data of selected volumes of interest (VOI) were obtained using a standardized procedure which was recently described in detail (*18*). Briefly, VOIs defined on MR images were aligned to the added PET radioactivity images interactively using an 'in house' data analysis tool. The biomedical image quantification software PMOD version 2.75 (PMOD Technologies, Zürich, Switzerland) was used for the kinetic analysis of the time-radioactivity curve (TACs) of the regional standardised uptake values (SUV=radioactivity per cubic centimeter VOI/(injected dose/body weight)).
The general model for the description of the binding of PET ligands to drug binding sites was introduced by Mintun et al. (*19*). In this study, only the simplified structures of the one- and two-tissue compartment models (*20, 21*) were used to describe the binding of the radioligand in the pig brain.
Depending on the model, the total radiotracer concentration measured with PET, $C_{PET}(t)$, can be described by:

$$C_{PET}(t) = (1 - V_b)C_T(t) + V_bC_{WB}(t) \quad \text{Eq. 1}$$
$$C_{PET}(t) = (1 - V_b)(C_{ND}(t) + C_S(t)) + V_bC_{WB}(t) \quad \text{Eq. 2}$$

where $C_{PET}(t)$ is the amount of radioactivity in 1 cm^3 brain tissue (one-tissue compartment model, equation 1). The nondisplaceable tracer concentration $C_{ND}(t)$ represents the sum of free $C_{FT}(t)$ and nonspecifically $C_{NS}(t)$ bound radiotracer in brain tissue and $C_S(t)$ the regional

concentration of the radiotracer specifically bound to the σ_1 receptors (two-tissue compartment model, equation 2). The fractional blood volume V_b describes the contribution of the whole blood radioactivity concentration $C_{WB}(t)$ to the PET signal. In this study V_b was fixed to 0.05 ml/cm^3.
The ordinary differential equations that describe the changes of radioactivity contents in these models are:
One-tissue compartment model (1TCM):

$$dC_T/dt = K_1C_a(t) - k_2" C_T (t) \quad \text{Eq. 3}$$

Two-tissue compartment model (2TCM):

$$dC_{ND}/dt = K_1C_a(t) - (k_2' + k_3')C_{ND}(t) + k_4C_S(t) \quad \text{Eq. 4}$$
$$dC_S/dt = k_3'C_{ND}(t) - k_4C_S(t) \quad \text{Eq. 5}$$

Three-tissue compartment model (3TCM):

$$dC_{FT}/dt = K_1C_a(t) - (k_2 + k_3 + k_5)C_{FT}(t) + k_4C_S(t) + k_6C_{NS}(t) \quad \text{Eq. 6}$$
$$dC_{NS}/dt = k_5C_{FT}(t) - k_6C_{NS}(t) \quad \text{Eq. 7}$$
$$dC_S/dt = k_3C_{FT}(t) - k_4C_S(t) \quad \text{Eq. 8}$$

The rate constants for the blood-brain and brain-blood transfer (K_1 and k_2' or k_2"), and the rate constants for the specific binding (k_3' and k_4) were estimated by nonlinear least-squares fits of the decay-corrected tissue time-activity curves and the arterial plasma concentration $C_a(t)$ of the radiotracer. Distribution volumes were calculated with both models to provide parameters related to transporter density. With the one-tissue compartment model, the respective parameter is the total distribution volume V_T (equal to $K_1/k"_2$). With the two-tissue compartment model the total distribution volume $V_T = V_{ND} + V_S$ [equal to $(K_1/k_2')(1 + k_3'/k_4)$], the specific distribution volume V_S [equal to $(K_1/k_2')(k_3'/k_4)$] and the binding potential $BP_{ND} = k_3'/k_4$ [equal to $f_{ND}B_{avail}/K_D$] provide measures of the specific binding, hence the σ_1 receptor density. B_{avail} is the concentration of unoccupied receptors available for the tracer, K_D is the equilibrium receptor-ligand dissociation constant and $f_{ND} = 1/(1+k_5/k_6)$ the free fraction of radiotracer in the nondisplaceable compartment depending on the nonspecific association and dissociation rate constants k_5 and k_6, respectively. A further important receptor dependent parameter is $k_3' = f_{ND}k_{on}B_{avail}$ where k_{on} describes the rate constant for forming the receptor-ligand complex [furthermore $k_4 = k_{off}$, $K_D = k_{off}/k_{on}$].
If in the 2TCM the rate constants k_2', k_3' are chosen as $k_2' = k_2/(1 + k_5/k_6)$ and $k_3' = k_3/(1 + k_5/k_6)$ the total distribution volumes of the 2TCM and 3TCM are identically $V_T = (K_1/k_2)(1 + k_3/k_4 + k_5/k_6)$. This also holds if in the 1TCM k_2" is chosen as $k_2" = k_2'/(1 + k_3'/k_4)$ and shows nicely the interdependence of the three different kinetic models. If there is a fast equilibration of tracer between the free and nonspecific tissue compartment – as it is normally assumed in the analysis of dynamic PET data – the 3TCM reduces kinetically to a 2TCM with one nondisplaceable compartment. If there is additionally a fast equilibration of tracer between the nondisplaceable and specific binding compartment, too fast to be seen on the time scale of dynamic PET, the 2TCM reduces further to a 1TCM and only K_1 and k_2" can be estimated from the data.
Goodness of fit of the different models was assessed using the F test and the Akaike information criterion (AIC) (*22, 23*). A significant improvement of the fit by use of model B instead of model A is indicated by F values of > 4.15 ($P < 0.05$) or AIC (model B) < AIC (model A).
Data are mean values ± standard deviation (SD). Coefficient of variation (COV) was calculated by mean/SD*100.

Supplemental information to Results

The normalised metabolite-corrected arterial plasma input function of (*S*)-(–)-^{18}F-fluspidine is significantly larger ($p<0.05$) than that of (*R*)-(+)-^{18}F-fluspidine (Fig. 1). Administration of SA4503 results in a significant increase of the (*R*)-(+)-^{18}F-fluspidine input ($p<0.05$).

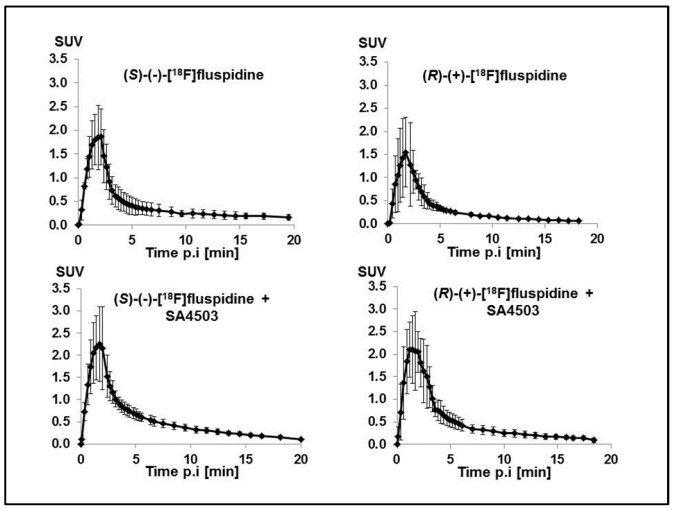

Figure 1. Metabolite-corrected arterial plasma imput function of (*S*)-(–)-^{18}F-fluspidine and (*R*)-(+)-^{18}F-fluspidine without and with administration of SA4503 (mean±SD).

The two radiolabelled enantiomers of ^{18}F-fluspidine were identified by comparing the retention time of *rac*-fluspidine as spiked solution (B in Fig. 2). Before, the polarimetric identification of the enantiomers of *rac*-fluspidine was performed in non-radioactive experiments using a chiral detector (OR-2090, JASCO, Germany; A in Fig. 2). The polarity of signal amplitudes obtained by the chiral detector was verified with (–)-vesamicol as reference compound.

Logan plot analysis (see Table 1) revealed a significant decrease after administration of SA4503 (whole brain (*S*)-(–)-^{18}F-fluspidine: -55%, (*R*)-(+)-^{18}F-fluspidine: -89%) was observed in all investigated regions.

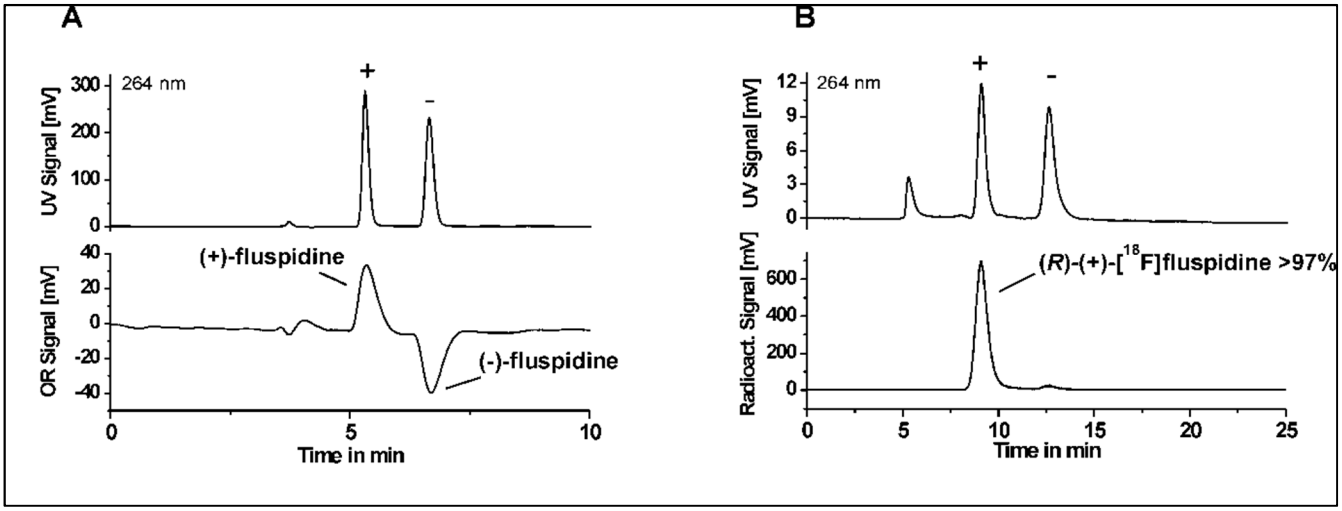

Figure 2. A) Chiral HPLC of *rac*-fluspidine using the chiral detector OR-2090 (conditions: Reprosil Chiral-OM; 90% n-hexane/10% isopropanol/0,1% diethyl amine; 1 mL/min); B) Chiral HPLC of (*R*)-(+)-^{18}F-fluspidine spiked with *rac*-fluspidine (conditions: Reprosil Chiral-OM; 95% n-hexane/5% isopropanol/0,05% diethyl amine; 0,75 mL/min).

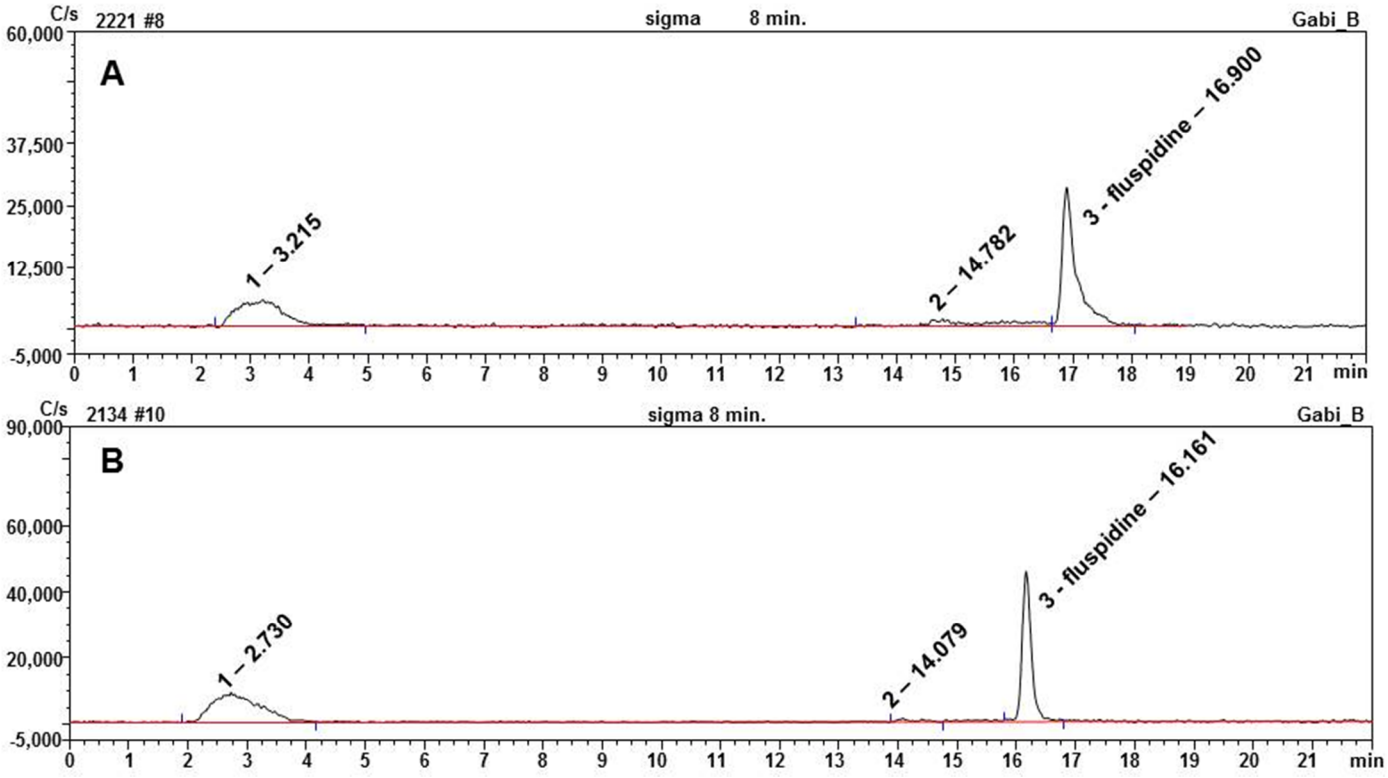

Figure 3. Radio-HPLC chromatograms of plasma samples obtained at 8 min after radiotracer injection for (A) (*S*)-(–)-^{18}F-fluspidine and (B) (*R*)-(+)-^{18}F-fluspidine.

TABLE 1

The total distribution volumes estimated by Logan plots of (*S*)-(–)-^{18}F-fluspidine and (*R*)-(+)-^{18}F-fluspidine in juvenile pigs with and without administration of SA4503.

Region	(*S*)-(–)-^{18}F-fluspidine		(*R*)-(+)-^{18}F-fluspidine	
	Control	+SA4503	Control	+SA4503
Front. cortex	9.8 ± 0.2	4.1 ± 1.7*	67.8 ± 25.9	7.4 ± 1.2*
Temp. cortex	12.2 ± 2.6	5.8 ± 2.9*	88.5 ± 43.3	9.2 ± 3.4*
Occ. cortex	13.1 ± 3.0	5.4 ± 3.0*	98.4 ± 49.2	9.0 ± 2.1*
Hippocampus	13.5 ± 2.8	6.0 ± 2.8*	95.2 ± 40.2	12.9 ± 7.5*
Striatum	13.5 ± 2.8	4.7 ± 2.7**	100.3 ± 46.3	7.0 ± 0.9*
Thalamus	14.1 ± 2.3	4.6 ± 2.4**	106.5 ± 47.6	6.9 ± 1.1*
Colliculi	15.2 ± 3.4	4.5 ± 2.7**	123.2 ± 59.2	6.7 ± 1.4**
Midbrain	15.4 ± 3.7	4.2 ± 2.5*	131.8 ± 58.8	6.2 ± 0.9*
Pons	15.2 ± 3.4	4.2 ± 2.8*	122.9 ± 54.6	6.9 ± 0.6*
Cerebellum	14.8 ± 3.9	5.0 ± 3.9**	140.8 ± 70.3	14.9 ± 10.2*

*$p<0.05$, **$p<0.01$

REFERENCES

1. Kekuda R, Prasad PD, Fei YJ, Leibach FH, Ganapathy V. Cloning and functional expression of the human type 1 sigma receptor (hSigmaR1). *Biochem Biophys Res Commun.* 1996;229:553-558.

2. Uchida N, Ujike H, Nakata K, et al. No association between the sigma receptor type 1 gene and schizophrenia: results of analysis and meta-analysis of case-control studies. *BMC Psychiatry.* 2003;3.

3. Satoh F, Miyatake R, Furukawa A, Suwaki H. Lack of association between sigma receptor gene variants and schizophrenia. *Psychiatry Clin Neurosci.* 2004;58:359-363.

4. Ishiguro H, Ohtsuki T, Toru M, et al. Association between polymorphisms in the type 1 sigma receptor gene and schizophrenia. *Neurosci Lett.* 1998;257:45-48.

5. Ohmori O, Shinkai T, Suzuki T, et al. Polymorphisms of the sigma$_1$ receptor gene in schizophrenia: An association study. *Am J Med Genet.* 2000;96:118-122.

6. Furuse T, Hashimoto K. Fluvoxamine for aripiprazole-associated akathisia in patients with schizophrenia: a potential role of sigma-1 receptors. *Ann Gen Psychiatry.* 2010;9:11.

7. Waterhouse RN, Collier TL. In vivo evaluation of [^{18}F]1-(3-fluoropropyl)-4-(4-cyanophenoxymethyl)piperidine: A selective sigma-1 receptor radioligand for PET. *Nucl Med Biol.* 1997;24:127-134.

8. Waterhouse RN, Lombardo I, Simpson N, Kegeles LS, Laruelle M. Evaluation of the novel sigma-1 receptor radioligand 1-(3-[F-18]Fluoropropyl)-4-[(4-cyanophenoxy)methyl]piperidine, [F-18]FPS: PET imaging studies in baboons. *Neuroimage.* 2000;11:S22.

9. Waterhouse RN, Nobler MS, Zhou Y, et al. First evaluation of the σ_1 receptor radioligand [^{18}F]1-3-fluoropropyl-4-((4-cyanophenoxy)-methyl)piperidine ([^{18}F]FPS) in healthy humans. *Neuroimage.* 2004;22:T29.

10. Mach RH, Gage HD, Buchheimer N, et al. *N*-[^{18}F]4'-fluorobenzylpiperidin-4yl-(2-fluorophenyl) acetamide ([^{18}F]FBFPA): A potential fluorine-18

labeled PET radiotracer for imaging sigma-1 receptors in the CNS. *Synapse.* 2005;58:267-274.

11. Kawamura K, Tsukada H, Shiba K, et al. Synthesis and evaluation of fluorine-18-labeled SA4503 as a selective sigma$_1$ receptor ligand for positron emission tomography. *Nucl Med Biol.* 2007;34:571-577.

12. Matsuno K, Nakazawa M, Okamoto K, Kawashima Y, Mita S. Binding properties of SA4503, a novel and selective σ_1 receptor agonist. *Eur J Pharmacol.* 1996;306:271-279.

13. Kawamura K, Ishiwata K, Tajima H, et al. Synthesis and in vivo evaluation of [^{11}C]SA6298 as a PET σ_1 receptor ligand. *Nucl Med Biol.* 1999;26:915-922.

14. Shiue CY, Shiue GG, Zhang SX, et al. *N*-(*N*-benzylpiperidin-4-yl)-2-[^{18}F]fluorobenzamide: a potential ligand for PET imaging of σ receptors. *Nucl Med Biol.* 1997;24:671-676.

15. Fujimura K, Matsumoto J, Niwa M, et al. Synthesis, structure and quantitative structure-activity relationships of σ receptor ligands, 1-[2-(3,4-dimethoxyphenyl)ethyl]-4-(3-phenylpropyl) piperazines. *Bioorg Med Chem.* 1997;5:1675-1683.

16. Lever JR, Gustafson JL, Xu R, Allmon RL, Lever SZ. σ_1 and σ_2 receptor binding affinity and selectivity of SA4503 and fluoroethyl SA4503. *Synapse.* 2006;59:350-358.

17. Brix G, Doll J, Bellemann ME, et al. Use of scanner characteristics in iterative image reconstruction for high-resolution positron emission tomography studies of small animals. *Eur J Nucl Med.* 1997;24:779-786.

18. Brust P, Zessin J, Kuwabara H, et al. Positron emission tomography imaging of the serotonin transporter in the pig brain using [^{11}C](+)-McN5652 and S-([^{18}F]fluoromethyl)-(+)-McN5652. *Synapse.* 2003;47:143-151.

19. Mintun MA, Raichle ME, Kilbourn MR, Wooten GF, Welch MJ. A quantitative model for the in vivo assessment of drug binding sites with positron emission tomography. *Ann Neurol.* 1984;15:217-227.

20. Koeppe RA, Holthoff VA, Frey KA, Kilbourn MR, Kuhl DE. Compartmental analysis of [^{11}C]flumazenil kinetics for the estimation of ligand transport rate and receptor distribution using positron emission tomography. *J Cereb Blood Flow Metab.* 1991;11:735-744.

21. Buck A, Gucker PM, Schönbächler RD, et al. Evaluation of serotonergic transporters using PET and [^{11}C](+)-McN-5652: assessment of methods. *J Cereb Blood Flow Metab.* 2000;20:253-262.

22. Akaike H. A new look at the statistical model identification. *IEEE Trans Automat Contr.* 1974;AC19:716-723.

23. Hawkins RA, Phelps ME, Huang SC. Effects of temporal sampling, glucose metabolic rates, and disruptions of the blood-brain barrier on the FDG model with and without a vascular compartment: studies in human brain tumors with PET. *J Cereb Blood Flow Metab.* 1986;6:170-183.